Journal of Applied Fluid Mechanics, Vol. 18, No. 1, pp. 73-86, 2025.
Available online at www.jafmonline.net, ISSN 1735-3572, EISSN 1735-3645.
https://doi.org/10.47176/jafm.18.1.2775

Simulation of the Separation of Homogeneous Whole Blood in a Spin-up Rotating Cylindrical Container

J. S. Fan[1], L. L. Xiao[†1], C. S. Lin[2], P. Wei [3]and K. X Zhang[4]

[1] *School of Mechanical and Automotive Engineering, Shanghai University of Engineering Science, Shanghai, China*
[2] *Artificial Intelligence Innovation and Incubation Institute, Fudan University, Shanghai, China*
[3] *School of Aerospace Engineering and Applied Mechanics, Tongji University, Shanghai, China*
[4] *School of Medicine, Nankai University, Tianjin, China*

†*Corresponding Author Email: xiaoll_sues@sues.edu.cn*

ABSTRACT

Centrifugal separation is a highly efficient technique for accelerating the sedimentation of blood constituents in a cylindrical container through high-speed spin-up rotation. Few studies have reported on the separation of different blood constituents from homogeneous mixture of whole blood. In this study, the process through which blood constituent sedimentation occurs in a spin-up rotating cylindrical container is numerically investigated. Whole blood is considered a homogeneous mixture of red blood cells (RBC) and plasma, which are both considered incompressible viscous liquids. The Euler multi-fluid VOF (volume of fluid) model is introduced to simulate the separation of RBCs and plasma. The effects of the rotation speed and the geometric construction of the cylindrical container on the sedimentation and stratification of different blood constituents are studied. A stable interface between the RBC layer and plasma layer forms earlier in a high position. With an increase in the rotation speed, the interface between the RBCs and plasma layers forms more quickly. In the cylindrical container with a helical groove on the outer wall, a stable vortex occurs near the groove, which forces red blood cells to move toward the lower location of the groove, resulting in a conical distribution of the RBC layer and a larger volume fraction of plasma near the exit at the top. This allows for sufficient precipitation of the plasma, improving the separation efficiency.

Article History

Received April 9, 2024
Revised July 5, 2024
Accepted August 1, 2024
Available online November 6, 2024

Keywords:

Blood separation
Euler multi-fluid VOF
Spin-up rotating cylinder
Rotation speed
Separation time

1. INTRODUCTION

Separating blood into different constituents for the purpose of storage or transfusion is a commonly performed medical procedure. Since the blood constituents–red and white blood cells–as well as platelets, which are suspended in plasma, have different densities, a common separation technique is to accelerate their sedimentation by centrifugation and then collect the different constituents individually.

This study is focused on the cylindrical containers that are crucial components of the blood centrifuges. Various cylindrical container structures are available, each affecting the flow field and subsequently impacting the movement of blood constituents. As a result, the cylindrical container construction plays a significant role in the separation of blood constituents. Figure 1 illustrates the specific mechanism for the separation of plasma. Blood is injected from the top and reaches the bottom of

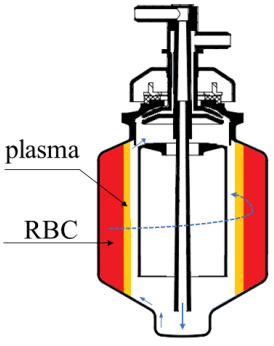

Fig. 1 Principle for the blood separation in a cylindrical container

the hollow cylindrical container through a vertical tube connected to the inlet of the container. The blood is separated into different constituents through centrifugal force. As the cylinder rotates at high speed, the denser red

blood cells are forced toward the outer wall and precipitate, allowing stratification of the blood. The plasma is collected at the top. This process ensures that the different blood components are separated effectively. The device is a few centimeters in diameter and rotates at several thousand revolutions per minute. The blood enters through the top and flows through the central channel, reaching the lower section of the centrifugation cylinder where sedimentation occurs. The walls rotate at a high angular velocity, causing the blood constituents to also rotate at the same high speed and precipitate during the process. The blood is transported upward along the inner wall by centrifugal force, and the different blood components are collected at the top.

Currently, the study of the phase separation process in a separator cylinder is limited to experimental observation. However, in recent years, numerical simulation methods have become an effective and economical means of studying the blood separation process. Computer Fluid Dynamics (CFD) has been widely used in blood flow and separation studies (Haghighi & Asadi Chalak, 2017; Haghighi & Aliashrafi, 2018). Previous numerical studies have often treated blood as a single-phase fluid, either a homogeneous Newtonian fluid or a non-Newtonian fluid with shear-thinning properties (Abugattas et al., 2020; Haghighi et al., 2020; Han et al., 2022; Li et al., 2023). To study the process of blood separation, blood must be considered a multiphase fluid. Two models can be applied to simulate multiphase blood: the first model considers RBCs to be pseudo-fluid and is typically simulated using the Euler-Euler two-fluid method and blood flow is generally simulated using the Eulerian-Eulerian two-fluid approach (Huang et al., 2009; Jung & Hassanein, 2008; Yilmaz et al., 2011; Qiao et al., 2019). The second model regards RBCs as suspended particles in blood, which more accurately reflects the effect of RBC deformation on hemodynamics. The first model is typically utilized for hemodynamic analysis in vessels with large diameters. In contrast, due to the large computation consumption required by the second model, it is commonly used for simulating blood flow in capillary vessels. and microfluidic chips under low-flow conditions (Wu & Feng, 2013; Yin et al., 2013; Xiao et al., 2016; Ebrahimi & Bagchi, 2022).

In recent research on blood centrifuge devices, Schenkel et al. focused solely on the movement of the RBC phase within its collection zone, treating it as a single-phase liquid model (Schenkel et al., 2013). However, the process of separating the various constituents of the blood in the separation cylinder has not been studied in detail. In this study, the separation cylinder is not fully filled with blood during the separation process. Therefore, whole blood is considered to be separated as it is injected, resulting in the coexistence of a gas-liquid free surface with a multiphase fluid. When simulating the separation process, it is important to consider the multi-phase flow of blood, including the movement of interpenetrating and mutually soluble liquids, the separation of different constituents of the stratification, and the free surface of the liquid in contact with the air.

The Euler-Euler model is a widely used blood simulation method, that treats particle flow as a continuous fluid flow. However, the gas-liquid interface clarity obtained by this model is not as good as that of the Volume of Fluid (VOF) model. To prevent the interface diffusion induced by the Euler-Euler model, due to the empirical closures required in the averaged equations, the Euler-Euler method is combined with the VOF method in ANSYS Fluent, resulting in the Euler Multi-fluid VOF (MF-VOF) model used in this study.

When the MF-VOF model is used, the interaction between the air and blood will be simulated by the VOF interface tracking algorithm. Moreover, the interaction between the plasma and the RBCs is simulated by the Euler-Euler model, as the RBC are dispersed in the plasma. The MF-VOF model combines the advantages of both models. Therefore, theoretically, this coupled model can be used to the simultaneously study RBC motility behavior and liquid surface shape changes. The MF-VOF model has primarily been used for gas-liquid flows in mixed or transitional states, such as churn flow, plunging jet flow, intermittent flows, and other chemical industries (Shonibare & Wardle, 2015; Parsi et al., 2016; Akhlaghi et al., 2019). However, it has rarely been applied to blood simulation.

Chen et al. investigated complex multiphase flow in an industrial degasser using the MF-VOF model and compared it with the Euler and DPM-VOF models (Chen et al., 2019). The MF-VOF model accurately describes the dispersed interface, as well as the ladle and sharp interfaces, and is in good agreement with the experimental results. Meng et al. analyzed the spiral separator using the MF-VOF model and compared it with the Euler-Euler model (Meng et al., 2023). The MF-VOF model was determined to be more effective in describing the distinct boundary between the two phases and results consistent with previous literature were produces.

This paper presents a numerical simulation of the process of separating different components in separation cylinders with different structures. For the first time, The Eulerian multi-fluid VOF model is adopted to investigate the complex multiphase flow behavior in a separation cylinder. The simulation considers whole blood to be a mixed flow medium of RBC and plasma phases using the MF-VOF model. The effects of rotational speed and the outer wall structure of the separation cylinder on the plasma separation process are investigated, which can help to understand the separation mechanism of blood components in the separation cylinder.

2. MODELS AND METHODS

Blood is essentially a non-Newtonian fluid (Haghighi & Pirhadi, 2019), that exhibits non-Newtonian properties (e.g., shear thinning phenomena and viscoelasticity) mainly at lower shear rates (<100/s) (Ling et al., 2021; Kannojiya et al., 2021). It has been experimentally confirmed that blood can be modeled as a Newtonian fluid under high shear rate conditions. Therefore, blood is considered to be a multiphase Newtonian fluid inside a high-speed rotating separator cylinder. In this paper,

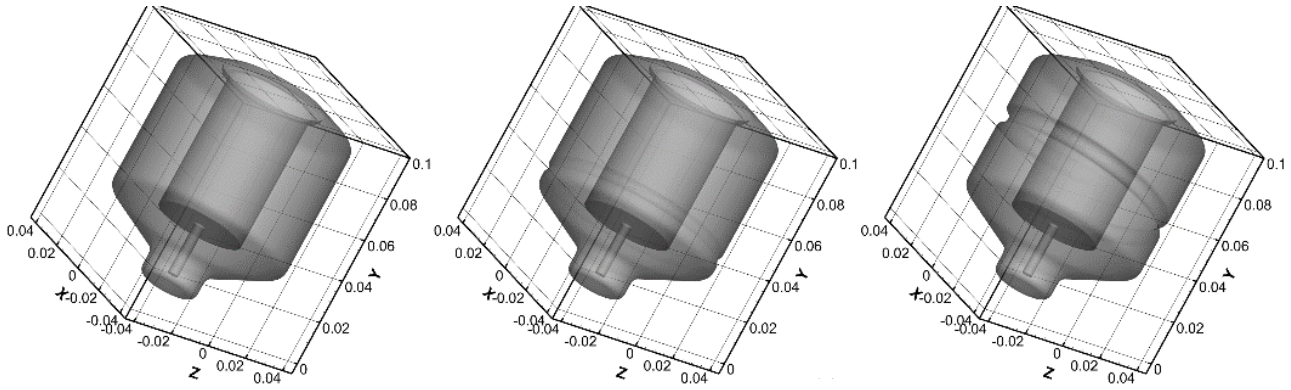

(a) (b) (c)

Fig. 2 (a) Smooth wall (b) Ring groove structure (c) Helical groove structure Separation cylinder geometry model

blood is considered as a fluid model consisting of two components, the RBC phase and the plasma phase, because blood still behaves as a liquid even at 98% RBC accumulation. In a previous study, blood had a mixed density of 1080 kg/m3 and a mixed viscosity of 0.0035 kg/(m-s) (Gijsen, 1999), and plasma had a density of 1000 kg/m^3 and a viscosity of 0.001 kg/(m-s) (Jung et al., 2006). Therefore, based on an RBC volume fraction of 45% (Dill & Costill, 1974), the density and viscosity of RBCs in the centrifugal environment were set to 1178 kg/m^3 and 0.0065 kg/(m-s), respectively, according to the weighted formula.

2.1 MF-VOF Mode

The MF-VOF model allows for the tracking of dispersed and sharp interfaces, while the continuous and discrete phases are treated as interpenetrating continua, still allowing for different velocity fields for each phase. The mass conservation equation and momentum conservation equation for each phase are given by the following equations:

The continuity equation is described as follows:

$$\frac{\partial}{\partial t}\left(\alpha_q \rho_q\right)+\nabla\cdot\left(\alpha_q \rho_q \overrightarrow{\upsilon_q}\right)=0 \tag{1}$$

The momentum equation in the Eulerian model is as follows:

$$\frac{\partial}{\partial t}\left(\alpha_q \rho_q\right)+\nabla\cdot\left(\alpha_q \rho_q \overrightarrow{\upsilon_q}\overrightarrow{\upsilon_q}\right)=-\alpha_q\nabla p-\nabla p_q+\nabla\cdot\overline{\overline{\tau_q}}+\alpha_q\rho_q\vec{g}+\overrightarrow{F_d} \tag{2}$$

$$\overline{\overline{\tau_q}}=\alpha_q\mu_q\left(\nabla\overrightarrow{\upsilon_q}+\nabla\vec{\upsilon}_q^{T}\right)+\alpha_q\left(\lambda_q-\frac{2}{3}\mu_q\right)\nabla\cdot\overrightarrow{\upsilon_q}\overline{\overline{I}} \tag{3}$$

where q stands for the different phases: p for plasma, a for air and r for RBC. α_q is the volume fraction of the phase; $\vec{\upsilon}$ is the velocity vector of the phase; ρ is the material density of the phase; g is the gravitational acceleration; is the pressure that the phases share together; F_d is the interphase trailing force.

In the Euler-Euler model, each computational cell is occupied by interpenetrating phases whose total volume fraction is equal to 1.

$$\sum\alpha_i=1 \tag{4}$$

The interphase traction force exerted between two liquid phases is calculated by the Schiller and Naumann model:

$$F_d=-\frac{3\alpha_p\alpha_r\rho_p C_d}{4d_r}\left|\vec{u}-\vec{u}\right| \tag{5}$$

The drag coefficient *Cd* is given by the following equation:

$$C_d=\begin{cases}\dfrac{24}{\mathrm{Re}}\left(1+0.15\,\mathrm{Re}_S^{0.687}\right), & \mathrm{Re}\ <1000\\ 0.44, & \mathrm{Re}\ \geq 1000\end{cases} \tag{6}$$

The relative Reynolds number Re is given by the following equation:

$$\mathrm{Re}=\frac{\rho\left|\vec{V}_r-\vec{V}_P\right|d_p}{\mu} \tag{7}$$

The mixture density and viscosity as a weighted sum of the volume fractions of both plasma and red blood cell phases are calculated as follows:

$$\rho_{mix}=\alpha_p\rho_p+\alpha_r\rho_r \tag{8}$$

$$\mu_{mix}=\alpha_p\mu_p+\alpha_r\mu_r \tag{9}$$

The VOF interface tracking model is used to describe the free liquid level between gas and liquid. Its continuity and momentum equations for the incompressible two-phase flow can be expressed as follows:

$$\nabla\cdot\left(\vec{v}\right)=0 \tag{10}$$

$$\frac{\partial\left(\rho_{mix}\vec{\upsilon}\right)}{\partial t}+\nabla\cdot\left(\rho_{mix}\vec{\upsilon}\vec{\upsilon}\right)=\nabla p+\nabla\cdot\left(\mu_{mix}\nabla\vec{\upsilon}\right)+\rho_{mix}\vec{g} \tag{11}$$

2.2 Geometric construction of the Cylinder

In this paper, we compare three types of separation cylinders with different outer walls. The main structure of the cylinder has the same dimensions and only the outer wall is partially optimized, as shown in Fig. 2. Figure 2(a)

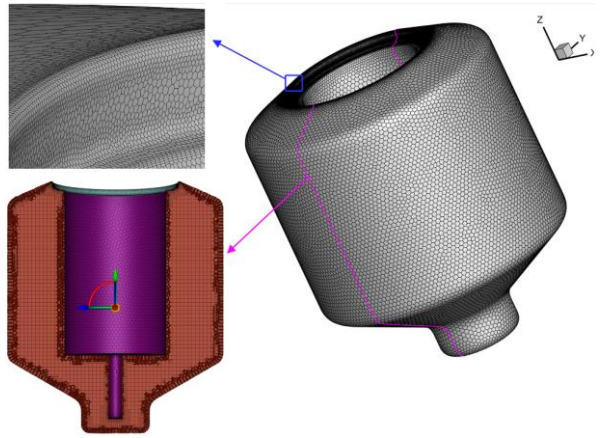

Fig. 3 Separation Cylinder Mesh

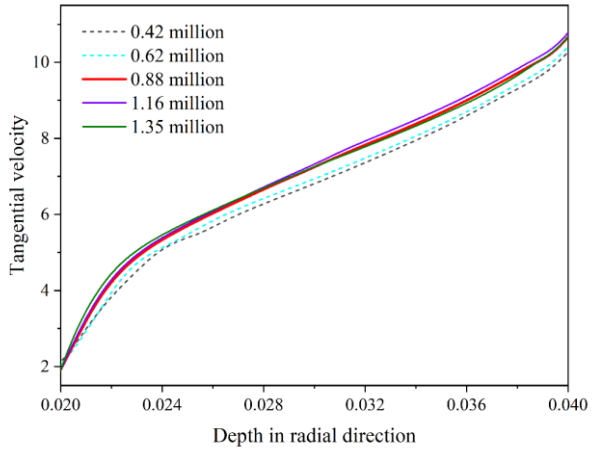

Fig. 4 Comparison of the tangential velocity with five different mesh densities

shows the separator cylinder structure with a smooth outer wall, and Fig. 2(b) shows a periodic ring groove at the bottom of the outer wall of the separator cylinder. Unlike Fig. 2(a) and (b), Fig. 2(c) shows a helical groove in the middle of the outer wall of the cylinder in the opposite direction of rotation. The meshing is carried out using Fluent's MESHING, while the Poly-Hexcore mesh type is used as shown in Fig.3, with a mesh count of 0.88 million and mesh refinement at local dimensions such as the top and the groove. Its unique polyhedral mesh is better suited to complex geometries. Compared to tetrahedral meshes, polyhedral meshes reduce the number of cells, which significantly reduces computation time. Five different densities of meshes are set up for the independence test. Figure 4 shows the tangential velocities obtained using five different density meshes at the same height and time. It is obvious that the change in the number of meshes is not significant when the number of meshes is greater than 0.88 million Therefore, 0.88 million are chosen as the number of grids for this simulation.

2.3 Simulation Setup and Modeling Parameters

Numerical simulations are performed using the computational fluid dynamics software ANSYS Fluent. SIMPLE pressure-velocity coupled format is used to solve the second order windward format with second order accuracy. Initially, the bottom of the container is occupied by the static mixed blood and the upper part of the container is full of air. The container is rotating acted by the centrifugal device while the blood is injected through the inlet. The separation process is transient and the blood flow is considered as a turbulent flow. The turbulence modeling is performed using SST k-ω, which is of higher accuracy in considering the transport of turbulent shear stress near the wall. The outer wall is set as a moving-wall with the lead axis as the rotational axis to simulate the rotational motion, and the rotational speed was 3000~5000 r/min. To ensure that each rotational cycle has enough computational steps to guarantee the computational precision (Dai et al., 2021), a step size of 10^{-4} s is set for the transient simulation. The RBCs are considered to be spherical particles with each having a diameter of 8×10^{-6}m spherical particles, given a velocity inlet of 0.5 m/s and RBC volume fraction of 45%. The outlet is defined as the outflow. The residual value used as a convergence criterion in this study was 10^{-3}。

2.4 Validation of Feasibility

Due to the lack of experimental data available for validation in previous studies on centrifugal devices. Therefore, the free liquid surface height obtained from the simulation at speed of 300 rpm is compared with the free liquid surface height calculated by the isobaric surface formula in a rotating container with equal angular velocity, as shown in Fig. 5.

Isobaric surface formula is as follows:

$$z = \frac{\omega^2 r^2}{2g} \tag{12}$$

where z stands for the height of a point on the free liquid surface and r stands for the distance between this point and the axis of rotation.

It can be seen that the two curves converge roughly. Therefore, the results of this simulation are considered to be reliable.

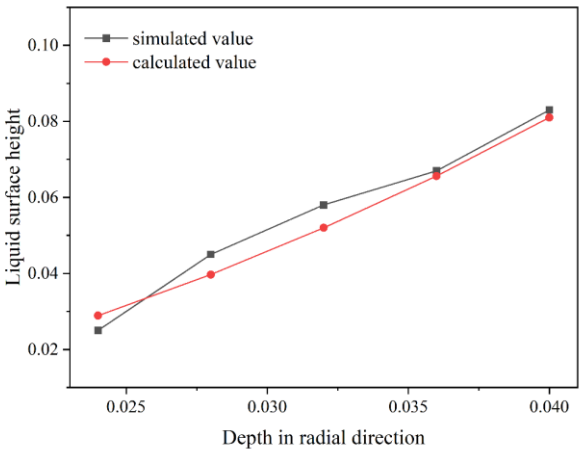

Fig. 5 Comparison of simulated free liquid level height and calculated free liquid level height

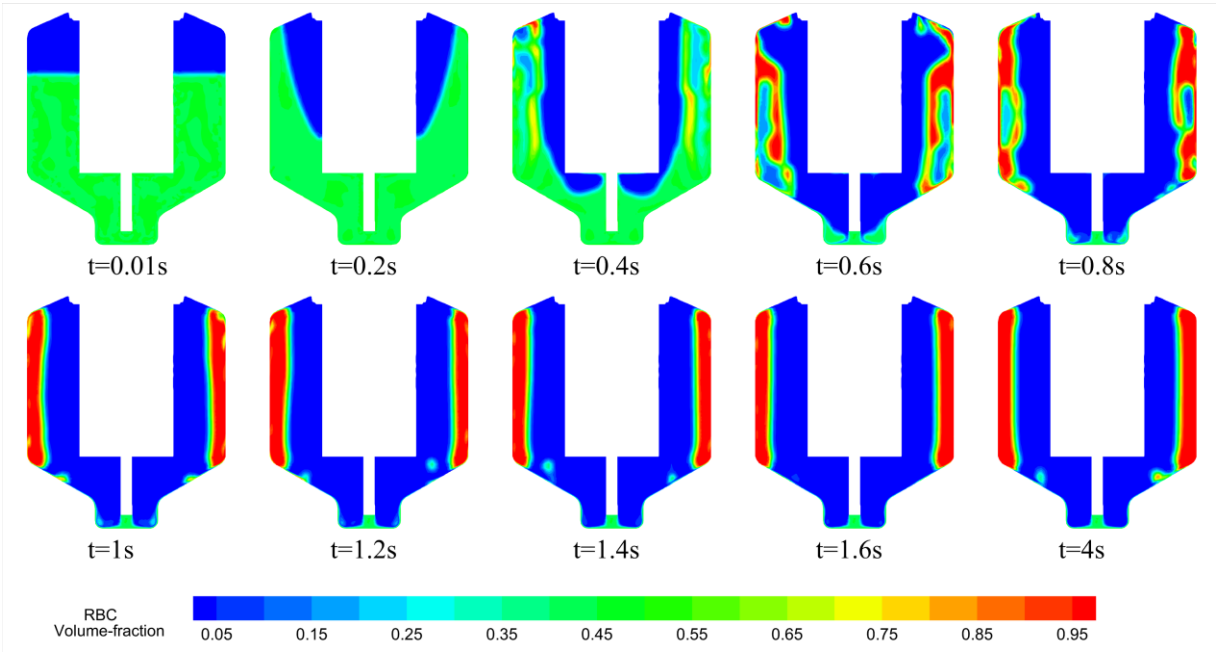

Fig. 6 Variation on distribution of RBC volume fraction of RBCs at different moments at the rotational speed of 3000 r/min in a cylinder with smooth outer wall structure

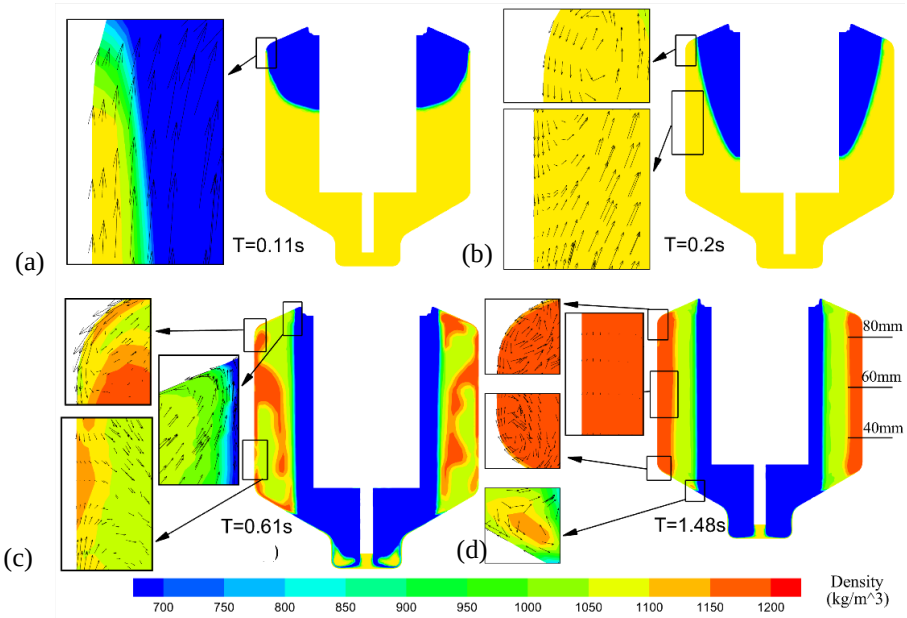

Fig. 7 Density mapping distributions and local velocity vectors at different moments (a) t=0.11s, (b) t=0.2s, (c) t=0.61s (d) t=1.48s of blood for separator cylinders with smooth outer wall structure at 3000r/min

3. RESULTS AND ANALYSIS

3.1 Whole Blood Separation in a Cylinder with a Smooth Outer Wall

The simulation involves the separation of whole blood into different constituents using a separator cylinder with a smooth outer wall structure as shown in Fig. 2(a). The separation cylinder is injected with whole blood at a height of h=0.07 m and rotated at a speed of 3000r/min. Figure 6 shows the volume fraction distribution of the RBC phase at different moments. At the initial time point, the RBCs and plasma are mutually soluble. The cylinder containing the blood sample begins to rotate around the central axis. The viscous nature of the blood causes it to be driven by the rotating outer wall thus following rotation. Under the influence of the centrifugal force, the liquid surface becomes parabolic from the horizontal surface and eventually approached the wall. At Fig. 6 t=0.4s, the RBCs are concentrated in the upper part of the separation cylinder, and then gradually separated from the blood, forming a clear stratified interface at t=1s, as shown in Fig. 6. During the period from the formation of the phase interface to the discharge of the plasma from the outlet, the distributions of the different constituents at the interface are relatively stable.

The cross-section at x=0 shows the density distribution of the blood and the local velocity vector distribution during the separation of the RBC phase from the plasma phase, as shown in Fig. 7. Initially, the wall

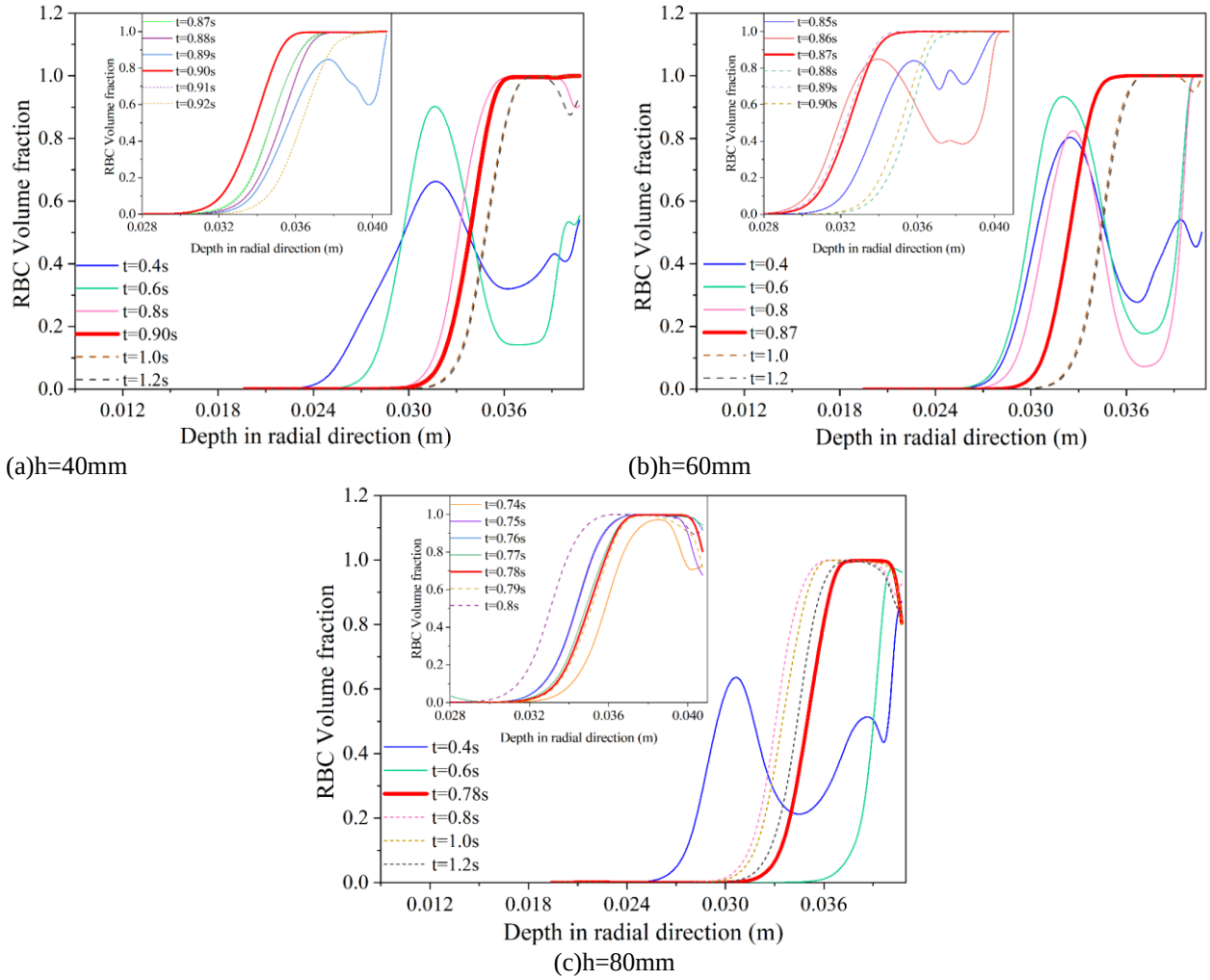

(a)h=40mm (b)h=60mm

(c)h=80mm

Fig. 8 Distribution of radial RBC volume fraction at different height positions

surface drives the liquid to rotate, forming a paraboloid on the whole blood surface, and the blood velocity vector is upward, as shown in Fig. 5(a). When the liquid surface touches the top wall, the fluid velocity near the wall turns downwards and forms a vortex on the top wall, as shown in Fig. 7(b). The downward fluid meets with the upward fluid from the bottom in the middle of the cylinder, causing a change in velocity direction. After a period of centrifugal action, all the blood is completely close to the outer wall surface of the separation cylinder, and the RBC first appear to separate in the upper part of the cylinder, as shown in Fig. 7(c). During the process of RBC precipitation, the internal flow field undergoes significant changes. The fluid moves upward, reaches the top, and then flows downward along the top wall. The upward velocity of the fluid from the bottom wall is restricted to the middle. When the phase interface stabilizes, the RBC phase and plasma phase inside the separator cylinder come to a relative rest with the outer wall. Vortices are observed at three turns inside the separator cylinder, as shown in Fig. 7(d). The bottom fluid injected from the inlet moves upward along the outer wall under centrifugal force to the already formed plasma layer. A sudden change in velocity leads to vortex and transient RBC separation.

To better characterize the separation efficiency, the period of time from the initial mixing state to the formation of a clear layered interface is defined as the separation time, which is denoted by $T_{separate}$. Therefore, the formation of the clear phase interface shown in Fig. 6 roughly infers that the separation cylinders with smooth structure are in the range of 0.8-1.0 s at 3,000 rpm.

Straight lines are drawn on the separation cylinder at different heights, as shown in Fig.7(d), the lines drawn at 40mm,60mm, and 80mm correspond to the bottom, center, and top, respectively. As the separation process proceeds, the volume fraction of RBCs at three different heights changes with time, and RBCs at the same height aggregate to the outside, which is reflected in the graph as the radial depth increases, the volume fraction of RBCs increases.

When the RBC volume fraction curve shows less fluctuation and no abrupt change, the separation tends to stabilize, that is, a clear stratified interface appears. As shown in Fig. 8, the curves for heights h=40mm and h=60mm fluctuate very little after 1.0s, representing $T_{separate}$ between 0.8s-1.0s, and the curve of h=80mm is almost unchanged after 0.8s, representing $T_{separate}$ between 0.6s-0.8s, which is consistent with the results shown in Fig.3. As shown in Fig.8, by comparing the details of volume distribution between the smallest time periods

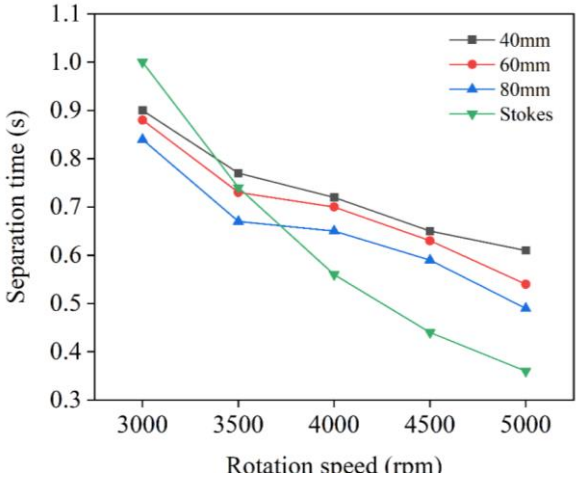

Fig. 9 Separation time for the blood at three height levels under different rotational speeds and RBC sedimentation time estimated by Stokes formula

within 0.2s, it is concluded that at 40mm $T_{separate}$ is approximately equal to 0.90s, at 60mm $T_{separate}$ is approximately equal to 0.87s. at 80mm $T_{separate}$ is approximately equal to 0.78s.

Following the stabilization of the stratification interface, a decrease in the volume fraction of RBCs near the wall at h = 80 mm is observed, as shown in Fig. 8(c). This decrease is caused by the vortex located at the top of the separation cylinder in Fig. 6(d), which carries both plasma and RBCs near the wall surface. As a result, the volume fraction of RBCs decreases. Despite the presence of the vortex at the top, the phase separation time at a height of 80 mm is faster than that at the bottom and middle. The separation time becomes earlier as the height increases.

3.2 Effect of Rotational Speed on the Separation Time

The selection of the most suitable centrifugation speed for separation is influenced by various factors. While a strong centrifugal field can cause cell damage, the applied centrifugal force should also be sufficient to allow the cells to move through the medium. A centrifugal speed that is too low will significantly decrease the separation efficiency. To analyze the impact of rotational speed on the separation of various blood constituents, the separation process in a separation cylinder with smooth outer wall rotating at speeds between 3000 and 5000 r/min is investigated.

The sedimentation of spherical particles in stationary Newtonian fluids is generally described simply by Stokes' formula and is based on several key assumptions, including the spherical shape of the particles, the negligible effects of the fluid boundary, the fluid being stationery and Newtonian, and the negligible interactions between particles. Currently, there is no detailed theoretical description of the separation between different components of a fluid rotating at high speed in a separation cylinder. The main reason for the stratification of blood constituents in the separator cylinder is the centrifugal force generated by high-speed rotation. Although the process details differ, the settlement time in the separator cylinder can be roughly estimated by replacing the gravitational acceleration with a much larger centrifugal acceleration and the Stokes settling rate equation is as follows:

$$v = \frac{2(\rho_1 - \rho_2)ad^2}{9\mu} \tag{13}$$

where ρ_1 is the particle density, ρ_2 is the fluid density, the centrifugal acceleration $a = \omega^2 r$, r is the distance from the center of the plasma layer to the rotor axis, d is the particle diameter, and μ is the fluid viscosity. The thickness of the plasma layer is used to represent the distance traveled by the RBC particles to settle, which in turn is used to calculate the settling time and compare it to $T_{separate}$ as defined in Section 4.1. Figure 8 shows the curves of various rotational speeds at different height positions (h=40mm, 60mm, and 80mm) in the separation cylinder. The results indicate that the time for the formation of a stable RBC-plasma interface between the two phases decreases as the position of the blood in the separation cylinder increases. Additionally, the time for phase separation decreases as the rotational speed increases, which is consistent with the curves fitted to the formula of the Stokes settling time calculation.

3.3 Effects of the Geometric Structure of the Outer Wall of the Cylinder on Whole Blood Separation

3.3.1 Whole Blood Separation in the Cylinder with a Ring Groove on the Outer Wall

In this section, whole blood separation in the separation cylinder with a ring groove on the outer wall (see Fig. 2(b)) is simulated, in which the height of the initially injected blood is h=0.07m. Figure 10 illustrates the distribution of the volume fraction of the RBC at different moments during the separation process. When the cylinder rotates about its central axis at the speed of 3000r/min, the free liquid surface is gradually become concave upward and RBC separation still occurs in the upper part of the cylinder (see t=0.01s-0.4s in Fig. 10). An obvious fluid stratified interface is stably formed at t=0.8s, which is earlier than that for the whole blood separation in the cylinder with a smooth outer wall. However, the plasma is still not completely precipitated from the RBC layer, which exists near the ring groove and in the upper region.

Unlike the distribution of RBCs in the cylinder with a smooth outer wall, the uniform distribution of RBCs oscillates periodically in a cylinder with an annular groove on the outer wall (see t=1s-4s). This is due to the presence of the annular groove. As shown in Fig. 11, when the blood flows from the bottom of the cylinder at high speed to the lower region of the groove, the groove deflects the moving blood to the inner region and a vortex is generated near the groove. The location of this vortex is not fixed. When it appears in the lower part of the ring groove, it induces the plasma to roll up and enter the RBC layer. (see t=1.58s, t=1.64s, and t=1.68s). At t=1.59s-1.62s, the vortex moves upward, and transports the mixture of rolled-up plasma and RBCs. Simultaneously, due to the high-speed rotation and continuous separation, the re-

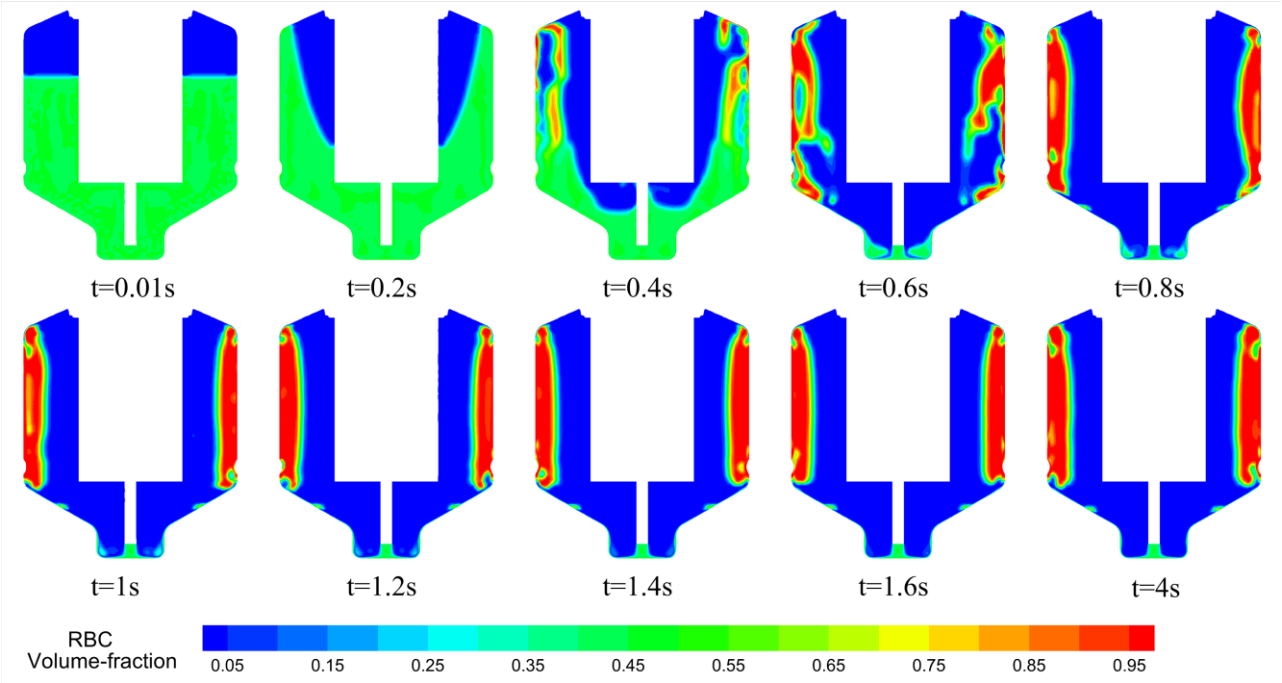

Fig. 10 Variation on distribution of the volume fraction of RBCs at different moments at the rotational speed of 3000 r/min in a cylinder with a ring-groove on the outer wall

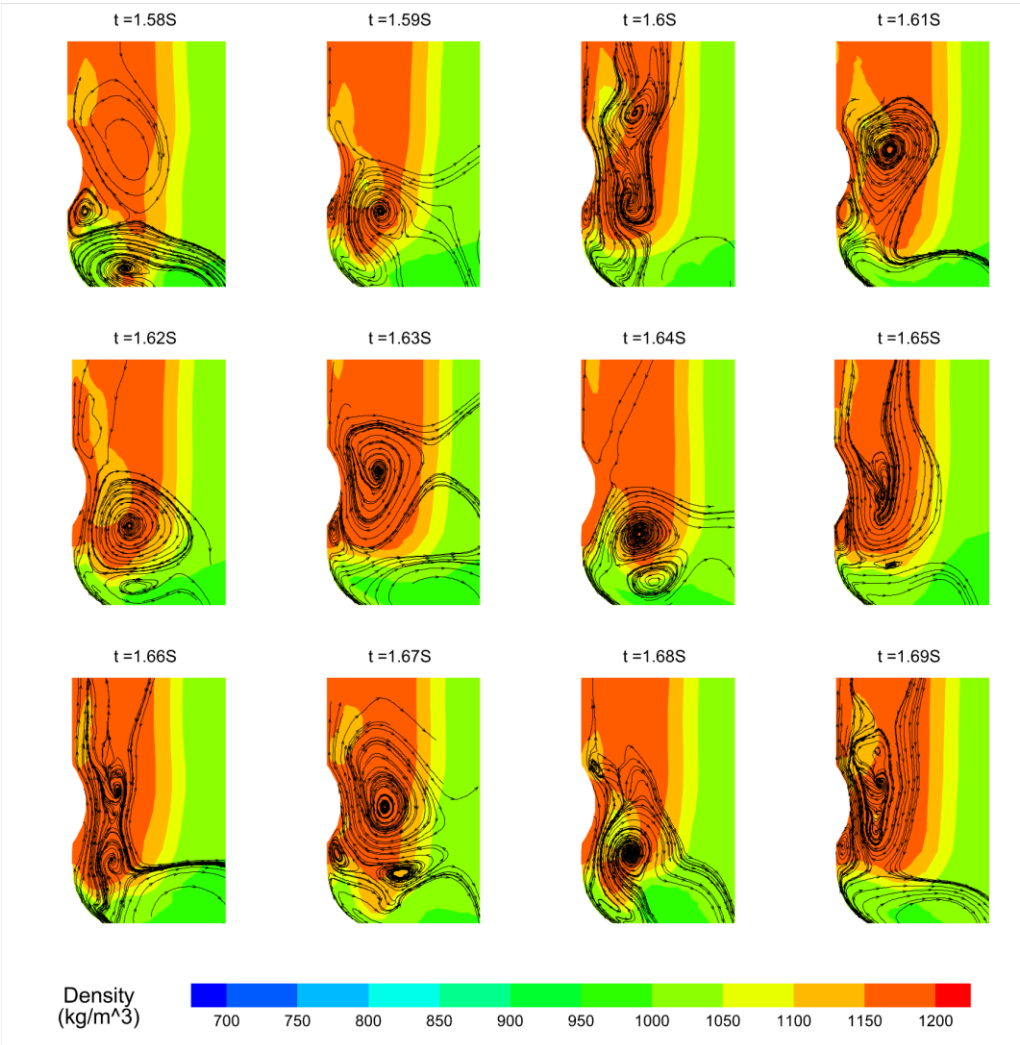

Fig. 11 Local velocity vector for the blood rotates about the central axis of the cylinder with a ring-groove on the outer wall at the speed of 3000r/min

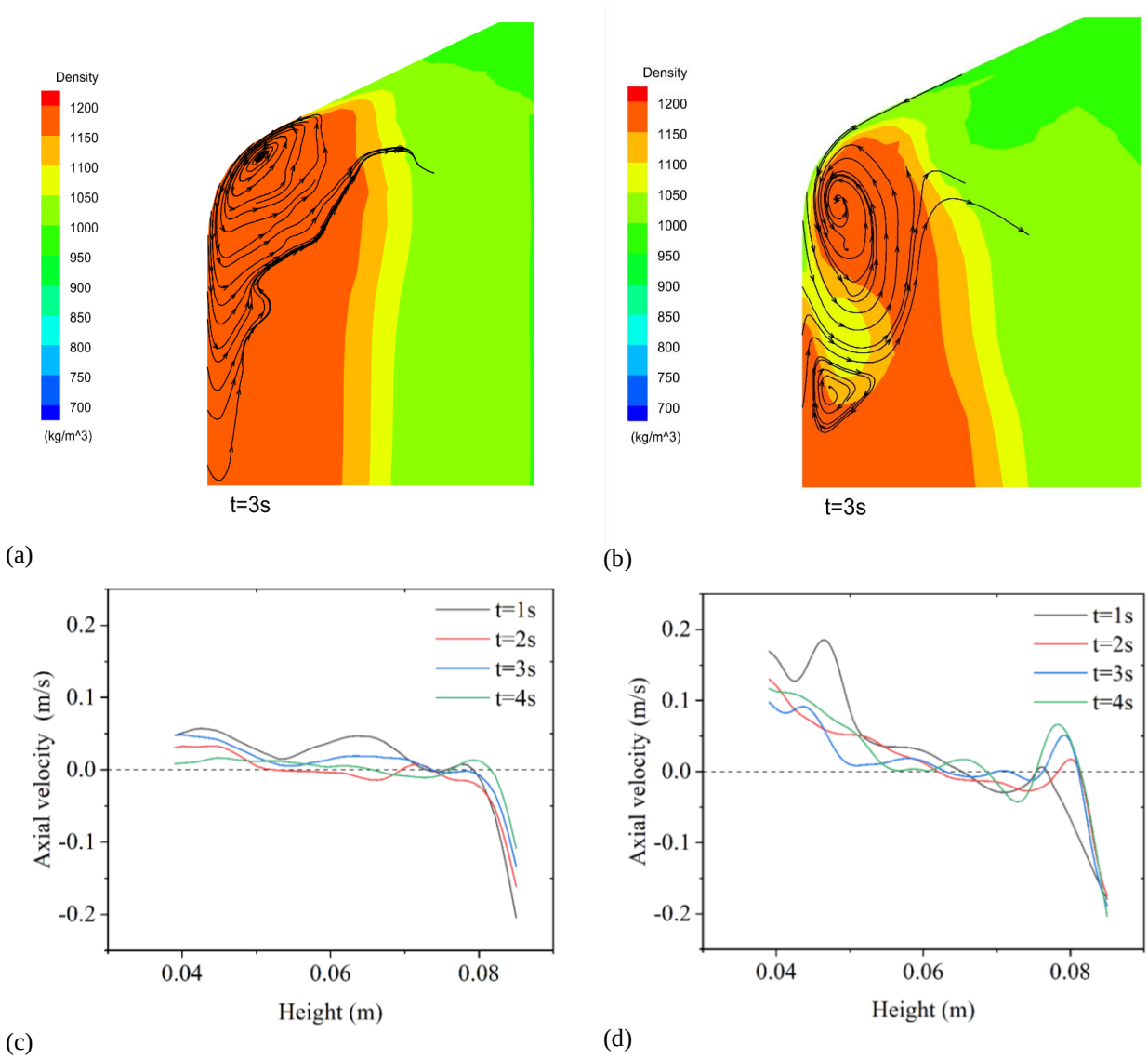

Fig. 12 Local density distribution and stream trace of the separator cylinders with smooth outer wall structure(a)and axial velocity distribution near the wall(c); Local density distribution and stream trace of the separator cylinders with ring outer wall structure(b)and axial velocity distribution near the wall(d)

mixed blood is pushed to the wall, causing the RBC volume fraction to gradually increase until separation is complete once again.

After the different constituents of the liquid are stratified and the interface is stabilized, an unprecipitated plasma appears in the upper region of the RBC layer (see Fig. 10). To clarify this finding, the local streamlines and density distributions in the top region near the outer wall of the separator cylinders with two different configurations are compared, as shown in Fig. 12. An obviously larger vortex is generated in the upper part of the cylinder with an annular groove on the outer wall, which causes the plasma near the top to infiltrate the cell layer, resulting in the phenomenon of plasma nonprecipitation in the cell layer. A further comparison of the profiles of the axial flow velocity for the fluid near the outer wall of the separation cylinders with the two different structures is shown in Figs. 12(c), and 12(d). Fig 12(c) shows that the axial flow velocity for the fluid in the container with a smooth outer wall decreases slowly with increasing height after the stratified interface is stabilized. As time elapses, it fluctuates slightly approximately 0, indicating that the liquid in the middle part of the container reaches equilibrium. Exceptionally, the liquid near the top flows downward, corresponding to the vortex in Figs 7(d) and 12(a). For the cylindrical container with an annular groove on the outer wall, the vortex generated near the annular groove structure (see Fig. 11) accelerates the liquid flow on the near-wall surface above the annular groove, the axial velocity for h=0.04m is larger in Fig. 12(d), by comparing with that in Fig. 12(c). It is likely that the presence of a counterclockwise vortex near the top causes a downward axial velocity. However, there is a small increase in the axial velocity below the vortex, which is mainly caused by the lower clockwise vortex. Under the combined effects of these two vortexes, the fluid in the middle part of the RBC layer moves toward the axis of the container, and the stronger entrainment of the vortexes leads to the infiltration of plasma into the RBC layer, as shown in Fig. 12(b).

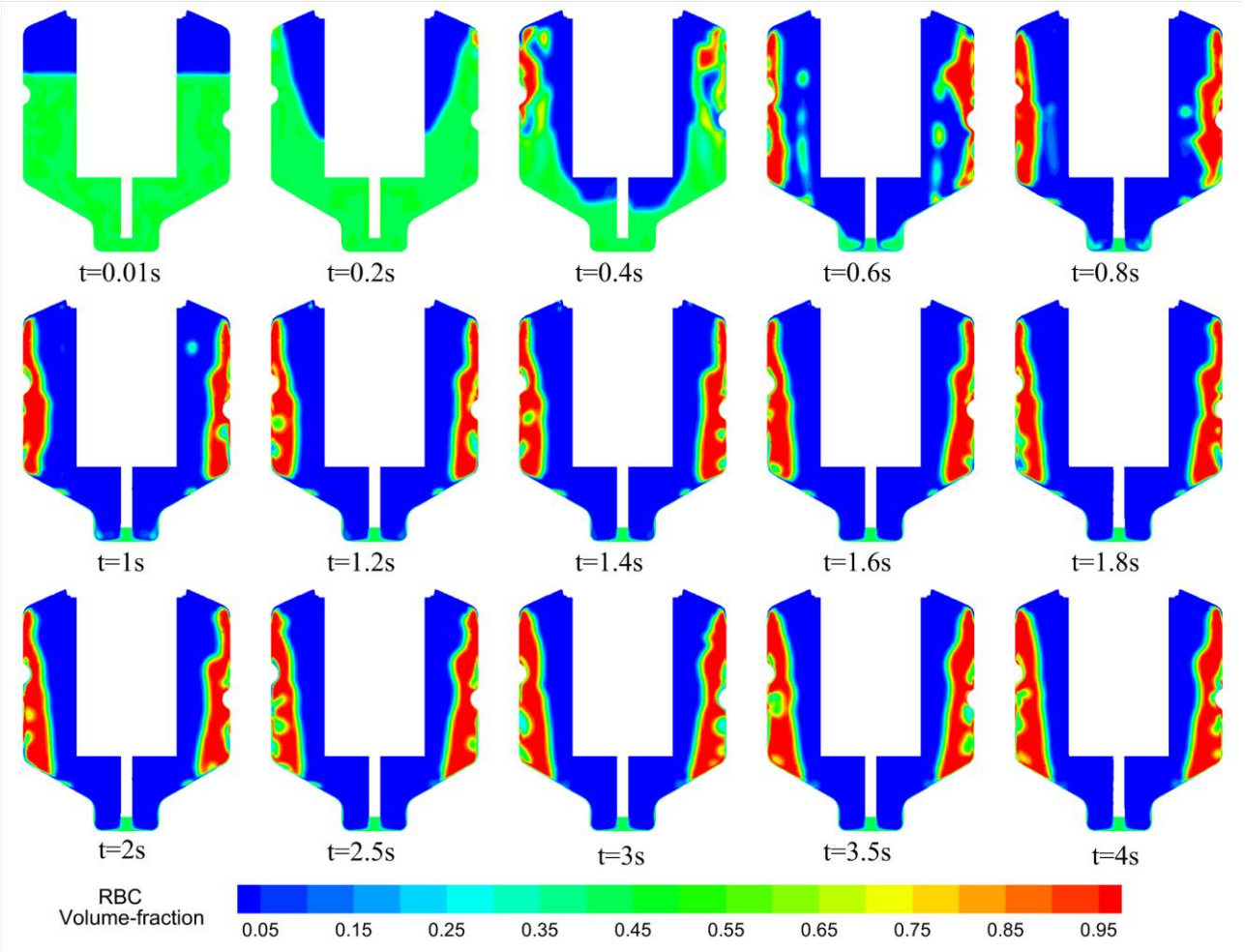

Fig. 13 Variation on the distribution of the volume fraction of RBCs for the blood separation in a cylinder with a helical groove on the outer wall at the rotational speed of 3000 r/min

3.3.2 Whole Blood Separation in the Cylinder with a Helical Groove on the Outer Wall

Finally, whole blood separation in the cylindrical container with a helical groove on the outer wall (see Fig. 2(c)) is analyzed. Similar to the flow in the containers with the above two structures mentioned above, the liquid surface initially deforms into a parabolic shape (refer to t=0.2s in Fig. 13). Then, the whole blood is gradually separated into RBCs and plasma. Moreover, RBCs appear near the outer wall in the upper part of the cylinder under the influence of centrifugal force (t=0.4s). However, the distribution of these two phases during separation are not symmetrical due to the asymmetrical distributions of the helical grooves on the outer wall (see t=0.6s-4s). In contrast to the stable phase interface formed in the container with a smooth outer wall and that with a symmetric ring groove on the outer wall, the stratified interface in this container gradually changes from an approximate plumb line to an oblique straight line inclined toward the outer wall. Additionally, red blood cells gradually accumulate in the lower part of the separation cylinder, resulting in narrow distribution at the top and a wide distribution at the bottom in the revolving section. Incomplete precipitation of plasma in the RBC layer also occurs near the helical groove.

After the stratified interface is formed, as the RBCs tend to move toward the outer wall, the RBCs layer becomes thicker. Due to the presence of the helical groove, a vortex is generated in the vicinity of the helical groove during the movement of the liquid inside the cylindrical container toward the wall, as illustrated in Fig. 14. And this vortex is relatively fixed, which is different from that induced by the ring groove, this vortex existing in the plasma layer transports the interior liquid upward, while that in the RBC layer transports the liquid near the wall downward. Therefore, RBCs are continuously deposited in the lower part of the helical groove, as shown in Fig. 14(c) and Fig. 14(d). Consequently, the RBCs distribution narrow at the top and wide at the bottom in the revolving section(x=0). The liquid transported downward by the helical groove collides with the whole blood injected from the bottom that is moving upward under centrifugal force. This collision forms two vortexes with different rotational directions, deflecting the velocity direction of the liquid located between the two vortexes toward the center of the container (refer to Figs. 14(e) and 14(f)). This phenomenon is similar to the incomplete precipitation of plasma in the bottom RBC layer that occurs in the containers of the two configurations mentioned in the above sections (refer to Figs 7(c) and 12(c)).

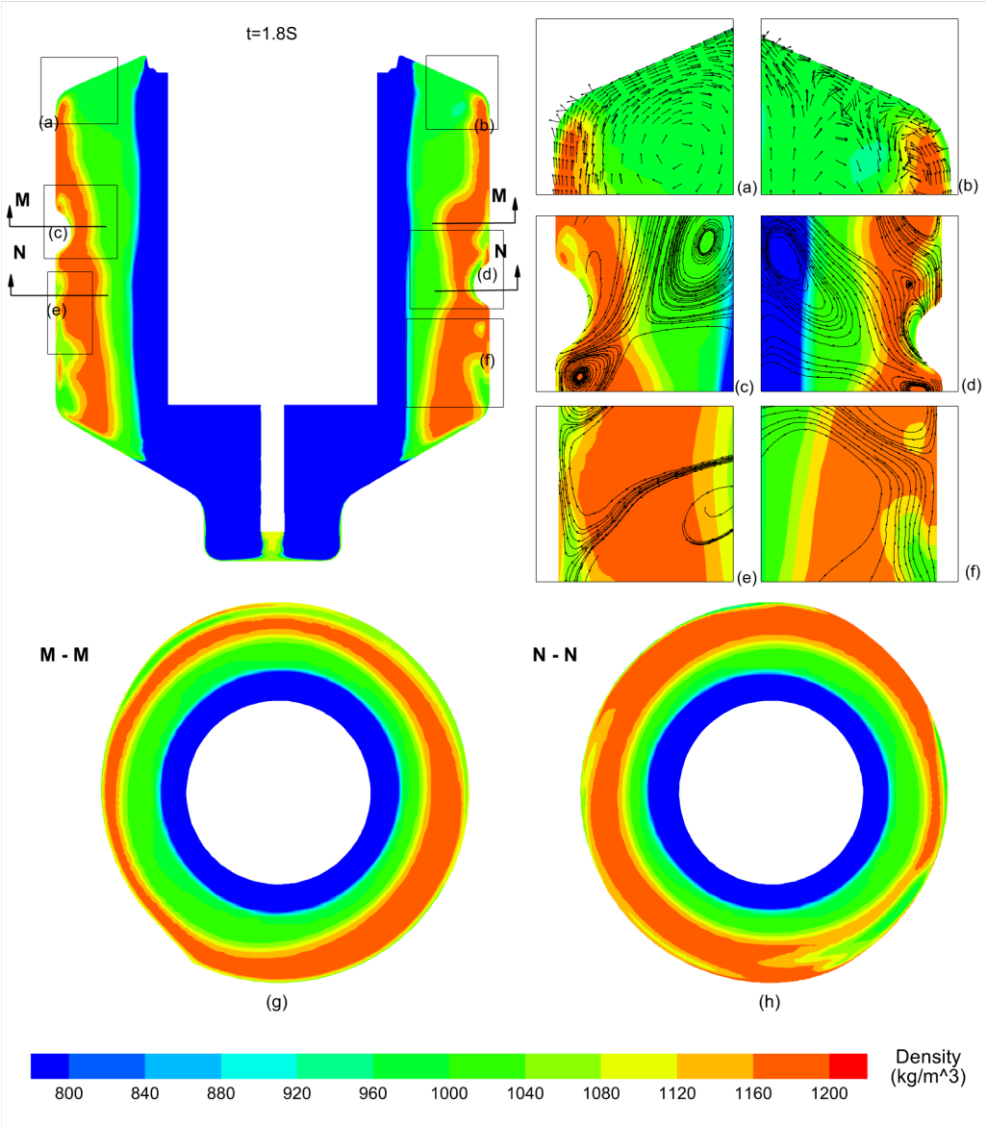

Fig. 14 Local density distribution and path line for the separation of blood in the cylindrical container with a helical groove in the outer wall

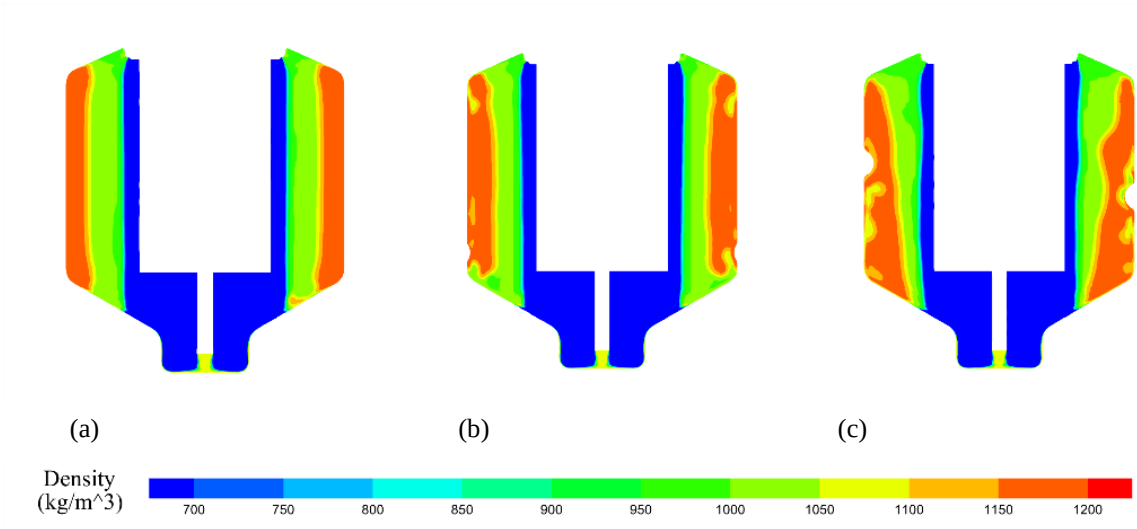

Fig. 15 Density distribution of the fluid in the cylindrical containers with three different structures when the separated plasma flows out of the outlet

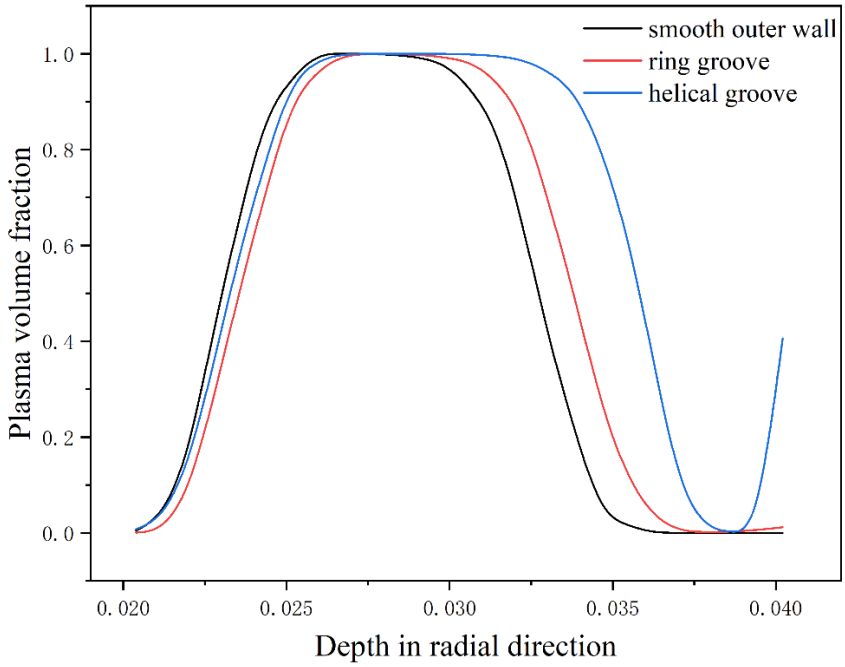

Fig. 16 Volume fraction of plasma in cylindrical containers with three different configurations at height of 0.085 m when the separated plasma flows out of the outlet

Finally, when the separated plasma flows out of the outlet, a comparative analysis of the density distribution of the fluid in the cylindrical containers with three different structures is given, as shown in Fig.15, this reveals that air occupies the central region inside the container, the denser RBC layer is located close to the wall, and the plasma layer is positioned between the air phase and the RBC layer. An obvious phase interface is formed between the air and plasma layers. The stratified interface between the RBC layer and the plasma layer agrees with the phase separation interface shown at t=4s in Fig. 6, Fig. 10, and Fig. 13. There is nearly no difference between the plasma layer distribution inside the container with a smooth outer wall and that inside the container with a ring groove on the outer wall. Both have an annular shape. However, the plasma layer distribution inside the container with a helical groove on the outer wall is cone shaped, wide at the top and narrow at the bottom. The plasma volume fractions of three different wall structures extracted at a height of 0.085m are shown in Fig. 16. It can be seen that changing the wall structure causes a change in the plasma volume fraction close to the outlet, which is highest in the spiral trough vessel. This structure facilitates efficient plasma collection at the outlet.

4. Summary and Conclusions

In this paper, the separation of blood plasma from a homogeneous whole blood in a spin-up rotating cylinder is numerically investigated by using Ansys Fluent software. Whole blood is regarded as a mixture of two mutually soluble incompressible viscous liquids, RBCs and plasma. The Eulerian multi-fluid VOF model is employed to simulate the sedimentation and stratification of different blood constituents. The effects of the rotational speed and the geometric configuration of the cylinder's outer wall on the process of plasma separation are investigated. The results show that under the strong centrifugal force, the sedimentation of RBCs occurs near the outer wall of the cylinder, and an obvious interface between the RBC layer and plasma layer first forms in the upper region of the cylinder. As the rotational speed increases, a stable fluid stratified interface forms earlier. The relationship between the time for the formation of a stable fluid stratified interface and rotational speed is presented, which is nearly consistent with the sedimentation time estimated by the Stokes formula. Moreover, in the cylinder with a ring-groove on the outer wall, the formation time of the RBC-plasma phase interface is shorter than that in the cylinder with a smooth outer wall, but the ring-groove structure could lead to nonuniform distribution of RBCs in the cell layer with. In the cylinder with helical groove on the outer wall, a stable vortex formed near the groove could continuously transport the RBCs to the lower part of the groove. Subsequently, the RBC layer has narrow distribution at the top and wide at the bottom in the revolved section, in other words, the RBC layer presents the shape of hollow truncated cone. Therefore, the plasma in the upper part of the cylinder can be fully precipitated, and the concentration of plasma at the outlet is higher, to improving the separation efficiency of the plasma.

Acknowledgments

This work is supported by the National Natural Science Foundation of China (Grant Nos. 11902188, 12002242), the Shanghai Science and Technology Talent Program (19YF1417400), and the Fundamental Research

Funds for the Central Universities. The grants are gratefully acknowledged.

CONFLICT OF INTEREST

The authors declare that they have no competing interests

AUTHORS CONTRIBUTION

J. S. Fan: Writing-original draft preparation,Data collection, Formal analysis. **P. Wei** and **C. S. Lin:** Writing-review and editing. **L. L. Xiao:** Supervision, Project administration. **K. X. Zhang:** Methodology.

REFERENCES

Abugattas, C., Aguirre, A., Castillo, E., & Cruchaga, M. (2020). Numerical study of bifurcation blood flows using three different non-Newtonian constitutive models. *Applied Mathematical Modelling*, *88*, 529–549. https://doi.org/10.1016/j.apm.2020.06.066

Akhlaghi, M., Mohammadi, V., Nouri, N. M., Taherkhani, M., & Karimi, M. (2019). Multi-Fluid VoF model assessment to simulate the horizontal air–water intermittent flow. *Chemical Engineering Research and Design*, *152*, 48–59. https://doi.org/10.1016/j.cherd.2019.09.031

Chen, G., Wang, Q., & He, S. (2019). Assessment of an eulerian multi-fluid VOF model for simulation of multiphase flow in an industrial Ruhrstahl–Heraeus degasser. *Metallurgical Research & Technology*, *116*(6), 617. https://doi.org/10.1051/metal/2019049

Dai, W. F., Wu, P., & Liu, G. M. (2021). A two-phase flow approach for modeling blood stasis and estimating the thrombosis potential of a ventricular assist device. *The International Journal of Artificial Organs*, *44*(7), 471–480. https://doi.org/10.1177/0391398820975405

Dill, D. B., & Costill, D. L. (1974). Calculation of percentage changes in volumes of blood, plasma, and red cells in dehydration. *Journal of Applied Physiology*, *37*(2), 247–248. https://doi.org/10.1152/jappl.1974.37.2.247

Ebrahimi, S., & Bagchi, P. (2022). A computational study of red blood cell deformability effect on hemodynamic alteration in capillary vessel networks. *Scientific Reports*, *12*(1), 4304. https://doi.org/10.1038/s41598-022-08357-z

Gijsen, F. J. H. Vosse, F. N. V. D., & Janssen, J. D. (1999). The influence of the non-Newtonian properties of blood on the flow in large arteries: steady flow in a carotid bifurcation model. *Journal of Biomechanics*, *32*(7), 705-713. https://doi.org/10.1016/s0021-9290(99)00014-7

Haghighi, A. R., & Aliashrafi, N. (2018). A mathematical modeling of pulsatile blood flow through a stenosed artery under effect of a magnetic field. *Journal of Mathematical Modeling*, *Online First*. https://doi.org/10.22124/jmm.2018.9259.1137

Haghighi, A. R., & Asadi Chalak, S. (2017). Mathematical modeling of blood flow through a stenosed artery under body acceleration. *Journal of the Brazilian Society of Mechanical Sciences and Engineering*, *39*(7), 2487–2494. https://doi.org/10.1007/s40430-017-0716-x

Haghighi, A. R., Aliashrafi, N., & Asl, M. S. (2020). An implicit approach to the micropolar fluid model of blood flow under the effect of body acceleration. *Mathematical Sciences*, *14*(3), 269–277. https://doi.org/10.1007/s40096-020-00340-x

Haghighi, A., & Pirhadi, N. (2019). A Numerical study of heat transfer and flow characteristics of pulsatile blood flow in a tapered artery with a combination of stenosis and aneurysm. *International Journal of Heat and Technology*, *37*(1), 11–21. https://doi.org/10.18280/ijht.370102

Han, D., Leibowitz, J. L., Han, L., Wang, S., He, G., Griffith, B. P., & Wu, Z. J. (2022). Computational fluid dynamics analysis and experimental hemolytic performance of three clinical centrifugal blood pumps: Revolution, Rotaflow and CentriMag. *Medicine in Novel Technology and Devices*, *15*, 100153. https://doi.org/10.1016/j.medntd.2022.100153

Huang, J., Lyczkowski, R. W., & Gidaspow, D. (2009). Pulsatile flow in a coronary artery using multiphase kinetic theory. *Journal of Biomechanics*, *42*(6), 743–754. https://doi.org/10.1016/j.jbiomech.2009.01.038

Jung, J., & Hassanein, A. (2008). Three-phase CFD analytical modeling of blood flow. *Medical Engineering & Physics*, *30*(1), 91–103. https://doi.org/10.1016/j.medengphy.2006.12.004

Jung, J., Lyczkowski, R. W., Panchal, C. B., & Hassanein, A. (2006). Multiphase hemodynamic simulation of pulsatile flow in a coronary artery. *Journal of Biomechanics*, *39*(11), 2064–2073. https://doi.org/10.1016/j.jbiomech.2005.06.023

Kannojiya, V., Das, A. K., & Das, P. K. (2021). Simulation of blood as fluid: A review from rheological aspects. *IEEE Reviews in Biomedical Engineering*, *14*, 327–341. https://doi.org/10.1109/RBME.2020.3011182

Li, Y., Wang, H., Xi, Y., Sun, A., Deng, X., Chen, Z., & Fan, Y. (2023). Impact of volute design features on hemodynamic performance and hemocompatibility of centrifugal blood pumps used in ECMO. *Artificial Organs*, *47*(1), 88–104. https://doi.org/10.1111/aor.14384

Ling, Y., Tang, J., & Liu, H. (2021). Numerical investigation of two-phase non-Newtonian blood flow in bifurcate pulmonary arteries with a flow resistant using Eulerian multiphase model. *Chemical Engineering Science*, *233*, 116426. https://doi.org/10.1016/j.ces.2020.116426

Meng, L., Gao, S., Wei, D., Zhao, Q., Cui, B., Shen, Y., & Song, Z. (2023). Particulate flow modelling in a spiral separator by using the Eulerian multi-fluid VOF

approach. *International Journal of Mining Science and Technology*, *33*(2), 251-263. https://doi.org/10.1016/j.ijmst.2022.09.016

Parsi, M., Agrawal, M., Srinivasan, V., Vieira, R. E., Torres, C. F., McLaury, B. S., Shirazi, S. A., Schleicher, E., & Hampel, U. (2016). Assessment of a hybrid CFD model for simulation of complex vertical upward gas–liquid churn flow. *Chemical Engineering Research and Design*, *105*, 71–84. https://doi.org/10.1016/j.cherd.2015.10.044

Qiao, Y., Zeng, Y., Ding, Y., Fan, J., Luo, K., & Zhu, T. (2019). Numerical simulation of two-phase non-Newtonian blood flow with fluid-structure interaction in aortic dissection. *Computer Methods in Biomechanics and Biomedical Engineering*, *22*(6), 620–630. https://doi.org/10.1080/10255842.2019.1577398

Schenkel, A., Deville, M. O., Sawley, M. L., Hagmann, P., & Rochat, J. D. (2013). Flow simulation and hemolysis modeling for a blood centrifuge device. *Computers & Fluids*, *86*, 185–198. https://doi.org/10.1016/j.compfluid.2013.06.019

Shonibare, O. Y., & Wardle, K. E. (2015). Numerical investigation of vertical plunging jet using a Hybrid Multifluid–VOF multiphase CFD solver. *International Journal of Chemical Engineering*, *2015*, 1–14. https://doi.org/10.1155/2015/925639

Wu, T., & Feng, J. J. (2013). Simulation of malaria-infected red blood cells in microfluidic channels: Passage and blockage. *Biomicrofluidics*, *7*(4), 044115. https://doi.org/10.1063/1.4817959

Xiao, L., Liu, Y., Chen, S., & Fu, B. (2016). Simulation of deformation and aggregation of two red blood cells in a stenosed microvessel by dissipative particle dynamics. *Cell Biochemistry and Biophysics*, *74*(4), 513–525. https://doi.org/10.1007/s12013-016-0765-2

Yilmaz, F., Kutlar, A. I., & Gundogdu, M. Y. (2011). Analysis of drag effects on pulsatile blood flow in a right coronary artery by using Eulerian multiphase model. *Korea-Australia Rheology Journal*, *23*(2), 89–103. https://doi.org/10.1007/s13367-011-0012-8

Yin, X., Thomas, T., & Zhang, J. (2013). Multiple red blood cell flows through microvascular bifurcations: Cell free layer, cell trajectory, and hematocrit separation. *Microvascular Research*, *89*, 47–56. https://doi.org/10.1016/j.mvr.2013.05.002